Structural Health Monitoring with Artificial Neural Network and Subspace-Based Damage Indicators

Marco M. Rosso[1](✉) , Angelo Aloisio[2] , Raffaele Cucuzza[1] ,
Dag P. Pasca[3] , Giansalvo Cirrincione[4] , and Giuseppe C. Marano[1]

[1] Politecnico di Torino, DISEG, Dipartimento di Ingegneria Strutturale, Edile e
Geotecnica, Corso Duca Degli Abruzzi, 24, 10128 Turin, Italy
{marco.rosso,raffaele.cucuzza,giuseppe.marano}@polito.it
[2] Università degli Studi dell'Aquila, Civil Environmental and Architectural
Engineering Department, via Giovanni Gronchi n.18, 67100 L'Aquila, Italy
angelo.aloisio1@univaq.it
[3] Norsk Treteknisk Institute, Børrestuveien 3, 0373 Oslo, Norway
dpa@treteknisk.no
[4] University of Picardie Jules Verne, Lab. LTI, Amiens, France
exin@u-picardie.fr

Abstract. In recent years, different structural health monitoring (SHM) systems have been proposed to assess the actual conditions of existing bridges and effectively manage maintenance programmes. Nowadays, artificial intelligence (AI) tools represent the frontier of research providing innovative non-invasive and non-destructive evaluations directly based on output-only vibration measures. This is one of the key aspects of smart structures of the future. In the current study, an artificial neural network (ANN) method has been proposed in order to perform damage detection based on subspace-based damage indicators (DIs) and other statistical indicators. A numerical case study example has been analysed with simulated damaged conditions. Based on a comparison between a reference situation and a new one, the greatest advantage in adopting these particular DIs is because they are able to point out significant changes, i.e. possible damage, without requiring a beforehand modal identification procedure, which may introduce further noise and modelling errors inside the traditional damage detection process.

Keywords: Structural health monitoring · Machine learning · Artificial neural network · Subspace-based damage indicators

1 Introduction

Many different Structural Health Monitoring (SHM) systems and innovative techniques have been proposed by the scientific community in recent years in order to assess the actual conditions, effectively manage maintenance programmes and increase the nominal life of existing heritage [1,2]. At least two

main different methodologies, which differ in the adoption or not of a model, can be identified into the SHM paradigm [3]. The first class of methods is denoted as *parametric* [4], whereas the second one is denoted as *non-parametric* [5]. Nowadays, the operational modal analysis (OMA) is the most widespread tool for dynamic identification of a structure based on output-only post-processing techniques of the vibration response [6,7]. The parametric Stochastic Subspace Identification algorithm (SSI) [8] and the non-parametric Enhanced Frequency Domain Decomposition (EFDD) [9] are the two most adopted OMA algorithms [3]. The SHM paradigm is structured into at least five levels of analysis, where the first four are associated with the diagnosis phase [10] and the last one to the prognosis phase [11]. The present study mainly focuses on Level 1 of the SHM problem, which is associated with the damage detection phase. This task could be possibly solved through the tracking of any change in the experimental modal parameters. However, several scholars proved that the OMA resulting modal parameters are not the best elements to solve the SHM Level 1 effectively [12]. Moreover, other studies provided non-parametric damage detection procedures which do not require a prior OMA, thus avoiding manipulating vibration data without a further introduction of modelling errors [13]. In particular, the subspace-based damage indicators (DIs) [14–16], rely on residuals calculated by covariance changes between two different situations: an initial reference condition and a current, possibly damaged, one. In the present study, a machine-learning artificial neural networks (ANN) model is adopted for the damage detection task (SHM Level 1) by exploiting information contained in raw vibration data combined with the above-mentioned subspace-based DIs, as depicted in Fig. 1. A similar procedure has already been attempted in [17], where both a support vector machine model and an ANN multi-layer percetron (MLP) architecture have been trained on a numerical pinned-pinned beam model to perform the damage classification task. The ANN has been trained on statistical parameters only directly calculated on the raw time series vibration data, such as mean, variance, skewness, kurtosis, etc. This promising study exploited very simple calculations and basic statistics to determine the input dataset of the MLP, without requiring any modelling assumptions or additional data manipulation. However, this method resulted in relatively poor accuracy on the simple numerical beam scheme, whereas accuracy negligibly improved on the analyzed real case studies. In the present work, the authors attempt to further enhance this MLP scheme by giving as input both the most important statistical features and even considering a subspace-based DI. Since this latter seems to be more sensitive to damage to the naive statistical indicators, their combination is expected to provide relatively higher accuracy in the classification performance. The current proposed damage detection framework with ANN and subspace-based DI has been finally analysed on a numerical simply supported beam case study model.
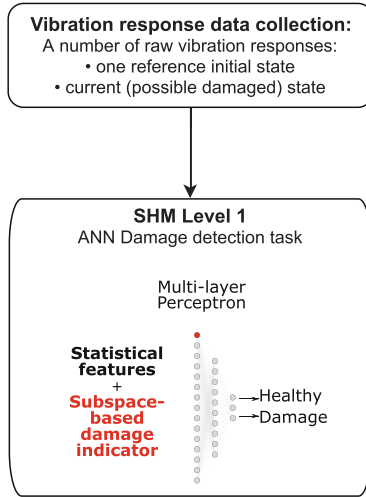
Fig. 1. Illustration of the proposed method to handle SHM Level 1 by an ANN trained on statistical features and subspace-based DI.

2   Subspace Residuals and Subspace-Based DIs

SSI is one of the most adopted algorithms in OMA and it relies on the following state-space representation [18]:

$$x_{k+1} = Ax_k + v_k$$
$$y_k = Cx_k + w_k \tag{1}$$

where $x_k \in \mathbb{R}^n$ are the states, whereas $y_k \in \mathbb{R}^r$ is the outputs, then $A \in \mathbb{R}^{n \times n}$ is called state transition matrix and $C \in \mathbb{R}^{r \times n}$ is denoted as observation matrix, with connoting n the system order and r the number of sensors. The term v_k represents a Gaussian white noise sequence with zero mean and constant covariance matrix $Q = \boldsymbol{E}(v_k v_k^T) \overset{\text{def}}{=} Q\delta(k - k')$ (with $\boldsymbol{E}(\cdot)$ as expectation operator), and represents the unmeasured environmental excitation, whereas the w_k terms is refereed to the measurement noise. Based on this state-space representation, different damage diagnosis indicators have been developed, which have the advantage of not requiring a prior OMA but directly working on output-only vibration data [19,20]. Tracking changes in time occurred in the above-mentioned features, the SHM Level 1 may be performed. Generally, the feature vector is approximately assumed as zero-mean normal Gaussian distributed in the reference state (assumed as an undamaged situation) which evolves in a non-zero mean when damages occur. Therefore, a residual vector may allow monitoring the relative changes among the new probable damaged state, and the initial reference one [21]. According to nomenclature proposed in [22], the subspace residuals are classified in *conventional* and *robust* with respect to how they are influenced by noise and changes in input excitation patterns. The residual matrix relies on

the orthonormal property between the subspaces related to a reference situation in comparison with the subspace related to a different structural response dataset, which could be varied because of input noise or structural damages. In [23, 24], a residual function based on the covariance-driven output-only subspace identification algorithm was proposed to detect damages directly from raw measurements $\boldsymbol{y}_k$ (e.g. acceleration responses). Let $G = \boldsymbol{E}(x_{k+1}y_k^T)$ be the cross-covariance between the states and the outputs, $R_i = \boldsymbol{E}(y_ky_{k-i}^T) = CA^{i-1}G$ be the theoretical output covariances, and

$$H_{p+1,q} \overset{\text{def}}{=} \begin{bmatrix} R_1 & R_2 & \dots & R_q \\ R_2 & R_3 & \dots & R_{q+1} \\ \vdots & \vdots & \ddots & \vdots \\ R_{p+1} & R_{p+2} & \dots & R_{p+q} \end{bmatrix} \overset{\text{def}}{=} Hank(R_i) \qquad (2)$$

the theoretic block Hankel matrix. Using measured data $(\boldsymbol{y}_k)_{k=1,\dots,n}$, a consistent estimate $\hat{H}_{p+1,q}$ is obtained from the empirical output covariances

$$\hat{R}_i = \frac{1}{N}\sum_{k=1}^{N} y_k y_{k-i}^T \qquad (3)$$

$$\hat{H}_{p+1,q} = Hank(\hat{R}_i) \qquad (4)$$

The residual function proposed by Basseville [23, 24] performs a comparison of the system undamaged or reference state with the damaged or current one. The system parameters in terms of eigenvalues and eigenvectors in the reference and current states are denoted respectively θ_0 and θ. [25] proposed a non-parametric damage detection approach in which it is not necessary to know explicitly the system parameters θ_0 in the reference state. In OMA SSI, the modal intrinsic properties information are obtained by the factorization property of the Hankel matrix which allows decomposing it in an observability matrix and a reversed controllability matrix [3]. The observability matrix is thus calculated starting from the Singular Value Decomposition (SVD) of the Hankel matrix:

$$\hat{H}_{p+1,q} \approx [\boldsymbol{U}_1\boldsymbol{U}_2] \begin{bmatrix} \boldsymbol{S}_1 & \boldsymbol{0} \\ \boldsymbol{0} & \boldsymbol{0} \end{bmatrix} [\boldsymbol{V}_1\boldsymbol{V}_2]^T \approx \boldsymbol{U}_1\boldsymbol{S}_1\boldsymbol{V}_1 \qquad (5)$$

As expressed in [26], $\boldsymbol{U}_1$ represents the left active subspace of the independent column vectors of the Hankel matrix, whereas $\boldsymbol{U}_2$ denotes the null subspace of the independent column vectors of the Hankel matrix. Similar definitions are provided for $\boldsymbol{V}_1$ and $\boldsymbol{V}_2$ for row vectors of Hankel matrix. Finally, $\boldsymbol{S}_1$ collects the non-neglectable singular values in a diagonal matrix sorted in decreasing order. The orthonormal properties of these matrices state that

$$\boldsymbol{U}_1^T \hat{H}_{p+1,q}\boldsymbol{V}_1 \approx \boldsymbol{S}_1 \qquad (6)$$

$$\hat{H}_{p+1,q}\boldsymbol{V}_2 \approx \boldsymbol{e}_V \qquad (7)$$

$$\boldsymbol{U}_2\hat{H}_{p+1,q} \approx \boldsymbol{e}_U \qquad (8)$$

The above residues $\boldsymbol{e}_V$ and $\boldsymbol{e}_U$ can be different from zero vectors because of noise effect or neglected weakly excited high modes. However, [26] pointed out that they are not the ideal candidates for tracking relative changes for damage detection purposes, taking into account the same state. The orthonormal property instead can be exploited by comparing two different states. Therefore, instead of using the null space $S(\theta_0^T)$ on the parameterized observability matrix [23,24], an empirical (non-parametric) null space S is computed on an estimated block Hankel matrix from data in the reference state using e.g. the SVD. The residue is thus expressed in matrix form as

$$\hat{\boldsymbol{e}}_c = S^T \hat{H}_{p+1,q} \tag{9}$$

where S^T is the left null space of the block Hankel matrix $\hat{H}_{p+1,q}$ in the reference state and $\hat{H}_{p+1,q}$ is the covariance block Hankel matrix in the current, possible damaged, one. In real life, the excitation covariance Q varies between different acquisition sessions due to random environmental noise, but the excitation is assumed as stationary during the same session. Therefore, a change in the excitation covariance Q leads to a change in the cross-covariance between states and outputs G and thus in the Hankel matrix. In [22,26], the authors presented a new residual definition, which appears to be robust to variations of excitation. Let $\hat{\boldsymbol{U}}_1$ be the matrix of the left singular vectors obtained from an SVD of $\hat{H}_{p+1,q}$. Since $\hat{\boldsymbol{U}}_1$ is a matrix with orthonormal columns, it is independent of the excitation Q. Therefore, the residual matrix can be written as

$$\hat{\boldsymbol{e}}_r = S \hat{U}_1^T \tag{10}$$

2.1   Yan et al. Damage Detection Test

In [26], the authors have provided a geometrical interpretation to the residual matrix concept, such as expression of a loss of orthonormality between reference subspace and another current state. Therefore, they give some DIs related to the rotation angle which arises between the two subspaces when structural damage occurs. Finally, they established that the best-found DI was given by the norm of matrix $\hat{\boldsymbol{e}}_r$

$$\hat{\sigma}_N^2 = norm(\hat{\boldsymbol{e}}_r) \tag{11}$$

where $norm(\bullet) : \mathbb{R}^{m \times n} \to \mathbb{R}$ denotes the matrix spectral norm operator which corresponds to the maximal singular value of a matrix, from the numerical point of view. Therefore, the authors adopt the following DIs:

$$I_{y,nr} = norm(\hat{\boldsymbol{e}}_c) \tag{12}$$

$$I_{y,r} = norm(\hat{\boldsymbol{e}}_r) \tag{13}$$

In the current study, this latter explained method has been selected as a subspace-based damage-sensitive feature to train the ANN classification model presented in Fig. 1.

3   Case Study: Numerical Beam Model

A numerical beam finite element (FE) model depicted in Fig. 2 has been analysed in the present study. It has been implemented into the *OpenSeesPy* module [27], and it represents a simply supported steel beam, with a square cross-section of side 0,10 m and a span length of 2,00 m. The steel material is characterized by Young's modulus $E = 210$ GPa and a mass density of $\rho = 7850$ kg/m^3. One beam support has been dynamically excited by a Gaussian random white noise acceleration [13]. This is a widespread method in the literature in order to simulate unknown environmental operational conditions in numerical cases or laboratory experiments [4,28]. The white noise process has been generated by a random sampling of a standard zero-mean Gaussian distribution $N(0,1)$, normalized and scaled up to 0.01 g of peak ground acceleration (PGA). Similarly to an acting earthquake limited to the vertical direction only, the input acceleration has been imposed in one single support to be sure to excite all modes, since any perturbation propagates almost instantaneously in every element of the beam [29]. The beam model has been discretized with a uniform mesh (see Fig. 3), in which the time history acceleration responses have been retrieved from in each node, simulating the presence of accelerometer sensors placed in correspondence of the nodes. To perform some initial comparisons, a critical situation
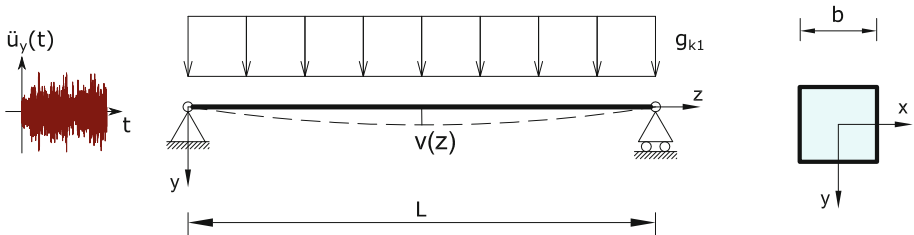

Fig. 2. Geometry of the simply supported beam with x, y, z reference system, where L is the span length, b is the square cross section side, g_{k1} is the self weight load and $v(z)$ is the beam deflection. $\ddot{u}_y(t)$ denotes the Gaussian white noise acceleration input.
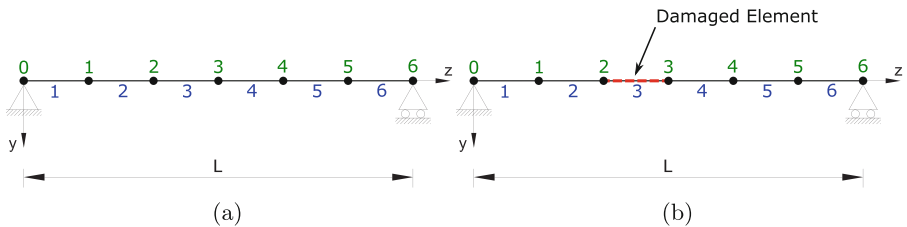

Fig. 3. Numerical beam FE model in the undamaged (a) and damaged (b) scenarios. In blue: element numbering; in green: node numbering.

in the damaged model has been considered with severe damage simulated with a cross-section reduction of 50% in a specific fixed position.

3.1   Limits of Traditional Modal Analysis and OMA

Since the availability of beam FE models in both in the damage and undamaged scenarios, it was possible to conduct an initial classic modal analysis in order to evaluate the dynamic properties changes. In Table 1, it is possible to point out a general increase of the natural periods due to the presence of the damage. This increase is strongly related to the modification of beam dynamic properties both related to a local flexural stiffness loss and a mass loss. By a visual inspection of the mode shapes, it is also possible to highlight qualitatively the loss of symmetry in the mode shapes due to the non-symmetric damage. In order to evaluate quantitatively the similarity between the mode shapes in the damaged and undamaged case, the cross modal assurance criterion (*crossMAC*), may be adopted:

$$\text{MAC} = \frac{\left|\hat{\phi}_U \hat{\phi}_D^T\right|^2}{\left|\hat{\phi}_U\right|^2 \left|\hat{\phi}_D\right|^2} \tag{14}$$

where $\hat{\phi}_U$ and $\hat{\phi}_D$ are the estimated mode shape vector referred to undamaged and damaged situations. Thereafter the mode shapes have been normalized, the crossMAC results have been reported in Table 2. Focusing on the main diagonal, it is worth noting a similarity of 99% among the first three mode shapes and it decreases to 96% on the fourth mode. On the other hand, focusing on

Table 1. Modal analysis comparison in the undamaged and damaged cases.

Mode	Undamaged case		Damaged case	
	T [s]	f [Hz]	T [s]	f [Hz]
1	0.534	1.872	0.611	1.638
2	0.134	7.479	0.139	7.184
3	0.060	16.722	0.064	15.680
4	0.049	20.583	0.052	19.368

Table 2. CrossMAC comparison in the undamaged and damaged cases.

		Undamaged case			
	Mode	1	2	3	4
Damaged case	1	0.9987	0.4359	0.5800	0.6245
	2	0.3948	0.9993	0.4281	0.4838
	3	0.5906	0.4112	0.9981	0.9535
	4	0.5768	0.3837	0.8866	0.9616

all off-diagonal elements, the cross-correlations between different modes in the two different situations are not of major interest within the scope of the present study. In conclusion, the traditional modal analysis cannot evidence the presence of damage, even with severe damage levels. Moreover, in real-life problems, it is not possible to perform a traditional modal analysis, since the damage type and location are unknown. However, even with performing an OMA, a damage detection framework merely based on frequency changes it would be quite ineffective. Furthermore, in real-life, background noise may jeopardize the entire identification process, preventing a reliable detection of decimal changes in natural frequencies and mode shapes. In addition, it is not simple, even for experts, to identify at first sight changes in mode shapes.

3.2 Influence of Damage Level and Acquisition Time Duration on Subspace-Based DIs

In this section, an empirical sensitivity analysis has been conducted on the beam FEM model to determine how the damage affects Yan's et al. [26] subspace-based DI. Referring to the undamaged and damaged scenarios illustrated in Fig. 3, to calculate the DI it is necessary to define the active space and null space dimensions. They can be identified by inspecting the singular values from SVD and detecting when they approach zero [3]. Thus, in this case, an active space dimension equal to two has been set. The time shift, adopted for Toeplitz matrix assembling, has been empirically set to 23 in order to contain the computational effort and still obtain an informative damage feature. Thereafter, an empirical study has been conducted in order to show the influence of the damage level percentage on the Yan et al. DI value for a certain identical input vibration and for the undamaged and damaged scenarios. Referring to Fig. 3, the damage level in element 3 has been varied from 5% to 50% of cross-section reduction with 5% constant step size. In Fig. 4 (a), even for low levels of damage, the subspace-based DIs point out the presence of damage assuming non-zero values in a monotonic
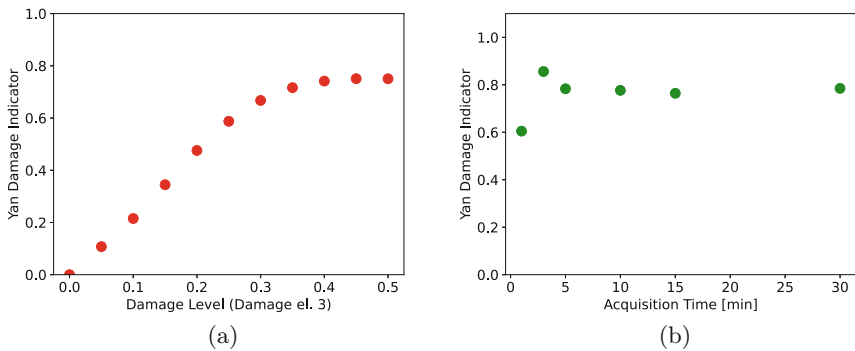

Fig. 4. Empirical study of parameters affecting the subspace-based DI: (a) analysis of the damage level percentage; (b) analysis of the acquisition time duration.

way. It assumes almost zero (order of magnitude 10^{-2}) only when there is no damage, and it approaches 1 with high level of damage. In conclusion, empirical analysis has been conducted regarding the acquisition time duration, considering 1, 3, 10, 15 and 30 min of time acquisition duration. In Fig. 4(b), the Yan et al. DI produces quite scatter values for very short acquisition durations and it stalls after the 5 min duration. Therefore, in the current study, an acquisition time of 5 min duration was addressed as the best trade-off between computational effort and subspace-based DI quality of information.

4   Damage Detection with ANN Multiclass Classification

In order to collect the dataset to perform ANN training to address SHM Level 1, in total, 5000 time histories numerical simulations were conducted on the above-mentioned beam FEM model. For every simulation, to increase the generalization of the proposed framework, the algorithm randomly selected how many elements considered damaged and the level of damage to assign to them accordingly three different levels: undamaged situation, low damage scenario (cross-section reduction of 25%) and high damage scenario (cross-section reduction of 50%). Thereafter, for each acceleration record, some statistical features have been extracted. In particular, as demonstrated in [17], the following statistical features appear to be the most informative and they can be effectively considered by a machine learning model for damage detection. Denoted in general each time series acceleration response as $\boldsymbol{x}$, the extracted features are the peak value $x_{\mathrm{P},(i,j)}$, the root mean square $x_{\mathrm{RMS},(i,j)}$, the variance $x_{\mathrm{VAR}(i,j)}$, the skewness $x_{\mathrm{SKEW},(i,j)}$, the kurtosis $x_{\mathrm{KURT},(i,j)}$, and the K-factor $x_{\mathrm{K},(i,j)}$.

$$x_{\mathrm{P},(i,j)} = \max\{|x_k|\}_{k=1}^{n}, \tag{15a}$$

$$x_{\mathrm{RMS},(i,j)} = \sqrt{\frac{1}{n}\sum_{i=1}^{n} x_k^2}, \tag{15b}$$

$$x_{\mathrm{VAR}(i,j)} = \frac{1}{n}\sum_{k=1}^{n}(x_k - \overline{x})^2, \tag{15c}$$

$$x_{\mathrm{SKEW}(i,j)} = \frac{\frac{1}{n}\sum_{k=1}^{n}(x_k - \overline{x})^3}{\left(\sqrt{x_{\mathrm{VAR}(i,j)}}\right)^3} \tag{15d}$$

$$x_{\mathrm{KURT}(i,j)} = \frac{\frac{1}{n}\sum_{k=1}^{n}(x_k - \overline{x})^4}{\left(\sqrt{x_{\mathrm{VAR}(i,j)}}\right)^4} \tag{15e}$$

$$x_{\mathrm{K},(i,j)} = x_{\mathrm{P},(i,j)} \cdot x_{\mathrm{RMS},(i,j)}. \tag{15f}$$

In the previous equations, the $\overline{x}$ indicates the mean value, the subscript $_k$ denotes the k-th component of the time series vector $\boldsymbol{x}$ which has totally n elements. The subscript $_i$ denotes the i-th simulation out of the 5000 total runs, whereas $_j$ denotes the j-th accelerometer from which the time series has been recorded.
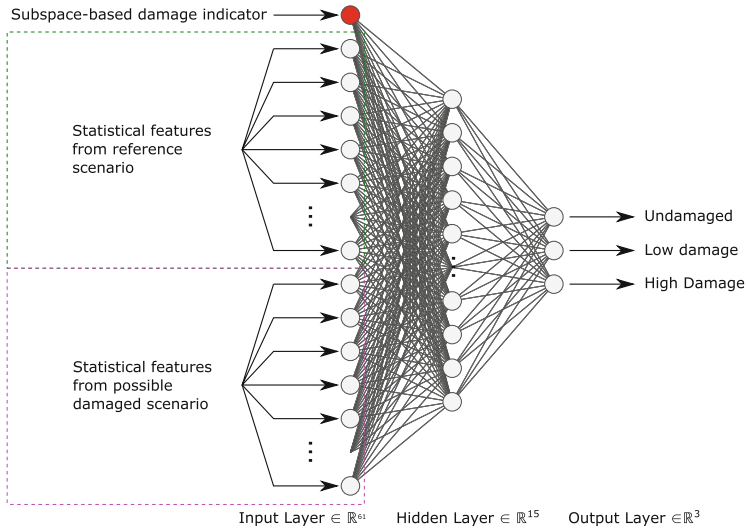
Fig. 5. Illustration of the implemented MLP ANN classification model, referring to the method (B) of Fig. 1.

Table 3. ANN MLP model summary. *None* indicates a variable dimension, depending on the batch size (in this case empirically set to 50).

Layer	Output shape	Activation function	Parameters number
Input Layer	(None, 61)	–	0
Hidden Layer	(None, 15)	ReLU	915
Output Dense Layer	(None, 3)	Softmax	48

Total Trainable parameters: 963
Epochs: 1000 (limited to 200 with Early Stopping)
Loss: Categorical Cross-entropy (Optimizer: Adam)

Because of 5 min acquisitions have been recorded for each run with a sampling frequency 500 Hz, n is thus equal to 150000. The number of accelerometers inside the beam domain is 5, excluding the extremal support restraint points. In total, for each numerical simulation, 6 statistical features have been extracted from each accelerometer producing, in total, 30 extracted features. Remembering that for each simulation, two cases have been considered (undamaged scenario and a possible damaged one), altogether, 60 features have been produced from each algorithm run. In the ANN architecture depicted in Fig. 5, the input is represented by 61 components coming from the statistical features concatenated with Yan's et al. subspace-based DI. The chosen architecture is a MLP with single hidden layer of 15 units, chosen as a good compromise between simplicity of the model, final accuracy performances and computational effort, trying to avoid overfitting and underfitting issues [30,31]. The summary of the MLP model
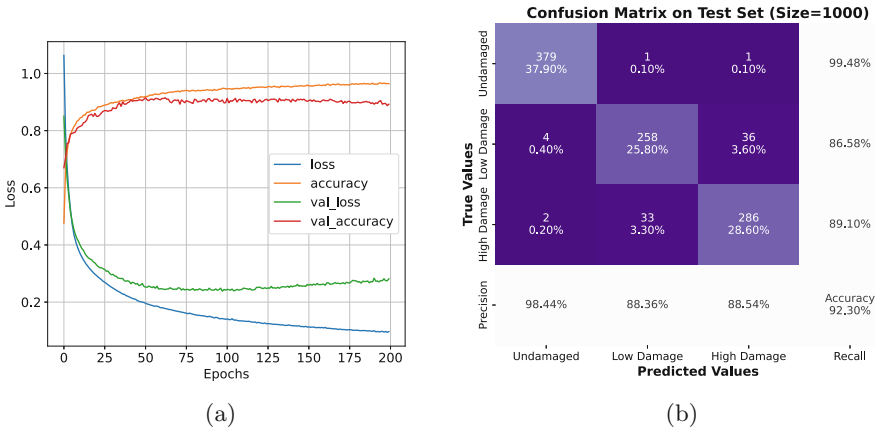
Fig. 6. MLP multiclass classification results for SHM Level 1. (a) Training performances history; (b) Confusion matrix of the test set predictions.

properties is reported in Table 3. The activation function of the hidden layer is the Rectified Linear Unit (ReLu) function, whereas the softmax activation function has been adopted in the output layer to deal with the multiclass classification task [30,31]. The MLP adopts the strategy *one-versus-the-rest* (or *one-versus-all*) to address the multiclass classification problem [31]. The entire dataset has been subdivided in a training set (80%), from which a further 10% has been adopted as validation set during the training phase, and a test set (20%). The maximum number of epochs has been set to 1000, but with the early stopping criterion [30] it was possible to stop at 200 epochs to avoid overfitting issues. The training history results are reported in Fig. 6(a). The performance of the trained model has been validated with the test set, whose classification results have been condensed in the confusion matrix illustrated in Fig. 6(b). The overall accuracy obtained is about 92.30% and it measures the portion of the validation set which has been correctly classified (the sum of main diagonal terms) out of the entire validation set size (1000 samples). Two other metrics are presented in the confusion matrix: precision and recall. The precision measures the number of samples correctly classified in a certain class over the total number of samples which have been associated with that class, whereas the recall represents the number of samples correctly classified to a certain class over the number of samples which actually belongs to that class [31]. In conclusion, the current MLP is able to provide quite interesting multiclass classification results considering the statistical time series features coupled with the Yan's et al. subspace DI, extending the capabilities of the MLP model trained in [17]. As a matter of fact, in that study, the MLP classification reaches only about 88% on the same numerical beam problem, whereas giving in input the new information contained in the subspace-based DI, the overall accuracy reaches 92.30%. Furthermore, a good generalization of the current ANN model is related to the fact that the 5000

numerical simulations randomly considered both how many damaged elements to take into account (even none) and the level of damage to associate with those selected elements.

5   Conclusions and Future Remarks

In the current study, the Level 1 of the ideal SHM paradigm, i.e. the damage detection task, is accomplished by an ANN model. The proposed method implements a MLP architecture to perform multiclass damage detection. A numerical beam FEM model has been analysed to simulate a realistic monitoring system placed on the structure to test the proposed method. In addition, some damaged scenarios have been considered by reducing the cross-section area of some elements in the model. The input data of the MLP are composed of statistical features calculated from time series vibration data. Furthermore, to enhance the classification performances of the MLP, a subspace-based damage sensitive feature is also combined with the input statistical features. After 5000 simulations, the ANN model has been trained and classification and generalization performances have been investigated reporting the results in a confusion matrix, inspecting the overall accuracy, the precision and the recall metrics. The results demonstrated that the Yan's et al. subspace-based DI helps to improve the MLP classification task reaching about 92.30% of overall accuracy. Future developments will explore the effects of the acquisition noise levels, which affect real-life applications. Further investigations may explore some other prominent deep learning architectures and experimentally prove the current study on a real engineering case study.

References

1. Singh, P., Keyvanlou, M., Sadhu, A.: An improved time-varying empirical mode decomposition for structural condition assessment using limited sensors. Eng. Struct. **232**, 111882 (2021). https://www.sciencedirect.com/science/article/pii/S0141029621000328
2. Marano, G., Quaranta, G., Monti, G.: Modified genetic algorithm for the dynamic identification of structural systems using incomplete measurements. Comput.-Aided Civ. Infrastruct. Eng. **26**(2), 92–110 (2011)
3. Rainieri, C., Fabbrocino, G.: Operational Modal Analysis of Civil Engineering Structures. Springer, New York (2014). https://doi.org/10.1007/978-1-4939-0767-0
4. Brincker, R., Ventura, C.E.: Introduction to Operational Modal Analysis. Wiley, Hoboken (2015)
5. Das, S., Saha, P., Patro, S.K.: Vibration-based damage detection techniques used for health monitoring of structures: a review. J. Civ. Struct. Heal. Monit. **6**(3), 477–507 (2016). https://doi.org/10.1007/s13349-016-0168-5

6. Brownjohn, J., Magalhaes, F., Caetano, E., Cunha, A.: Ambient vibration re-testing and operational modal analysis of the humber bridge. Eng. Struct. **32**(8), 2003–2018 (2010). https://www.sciencedirect.com/science/article/pii/S0141029610000878

7. Aloisio, A., et al.: Indirect assessment of concrete resistance from FE model updating and young's modulus estimation of a multi-span PSC viaduct: experimental tests and validation. Elsevier Struct. **37**, 686–697 (2022). https://doi.org/10.1016/j.istruc.2022.01.045

8. Peeters, B., De Roeck, G.: Reference-based stochastic subspace identification for output-only modal analysis. Mech. Syst. Signal Process. **13**(6), 855–878 (1999)

9. Brincker, R., Zhang, L., Andersen, P.: Modal identification of output-only systems using frequency domain decomposition. Smart Mater. Struct. **10**(3), 441 (2001)

10. Bernagozzi, G., Ventura, C.E., Allahdadian, S., Kaya, Y., Landi, L., Diotallevi, P.P.: Output-only damage diagnosis for plan-symmetric buildings with asymmetric damage using modal flexibility-based deflections. Eng. Struct. **207**, 110015 (2020). https://www.sciencedirect.com/science/article/pii/S0141029619314476

11. Rytter, A.: Vibrational Based Inspection of Civil Engineering Structures, vol. Fracture & dynamics, Vol. R9314 No. 44. Aalborg University, Department of Building Technology and Structural Engineering, Ph.D. thesis (1993)

12. Limongelli, M.P., et al.: Vibration response-based damage detection. In: Sause, M.G.R., Jasiūnienė, E. (eds.) Structural Health Monitoring Damage Detection Systems for Aerospace. SAT, pp. 133–173. Springer, Cham (2021). https://doi.org/10.1007/978-3-030-72192-3_6

13. Aloisio, A., Di Battista, L., Alaggio, R., Fragiacomo, M.: Sensitivity analysis of subspace-based damage indicators under changes in ambient excitation covariance, severity and location of damage. Eng. Struct. **208**, 110235 (2020)

14. Döhler, M., Hille, F., Mevel, L.: Vibration-based monitoring of civil structures with subspace-based damage detection. In: Ottaviano, E., Pelliccio, A., Gattulli, V. (eds.) Mechatronics for Cultural Heritage and Civil Engineering. ISCASE, vol. 92, pp. 307–326. Springer, Cham (2018). https://doi.org/10.1007/978-3-319-68646-2_14

15. Shokravi, H., Shokravi, H., Bakhary, N., Rahimian Koloor, S.S., Petrů, M.: Health monitoring of civil infrastructures by subspace system identification method: an overview. Appl. Sci. **10**(8) (2020). https://www.mdpi.com/2076-3417/10/8/2786

16. Yan, A.M., De Boe, P., Golinval, J.C.: Structural damage diagnosis by Kalman model based on stochastic subspace identification. Struct. Health Monit. **3**(2), 103–119 (2004)

17. Finotti, R.P., Cury, A.A., Barbosa, F.D.S.: An SHM approach using machine learning and statistical indicators extracted from raw dynamic measurements. Latin Am. J. Solids Struct. **16**(2) (2019)

18. Kvåle, K.A., Øiseth, O., Rønnquist, A.: Operational modal analysis of an end-supported pontoon bridge. Eng. Struct. **148**, 410–423 (2017). https://www.sciencedirect.com/science/article/pii/S0141029616307805

19. Döhler, M., Mevel, L.: Modular subspace-based system identification from multi-setup measurements. IEEE Trans. Autom. Control **57**(11), 2951–2956 (2012)

20. Döhler, M., Mevel, L., Zhang, Q.: Fault detection, isolation and quantification from gaussian residuals with application to structural damage diagnosis. Ann. Rev. Control **42**, 244–256 (2016). https://www.sciencedirect.com/science/article/pii/S1367578816300839

21. Allahdadian, S., Döhler, M., Ventura, C., Mevel, L.: Towards robust statistical damage localization via model-based sensitivity clustering. Mech. Syst. Signal Process. **134**, 106341 (2019). https://www.sciencedirect.com/science/article/pii/S088832701930562X

22. Döhler, M., Mevel, L., Hille, F.: Subspace-based damage detection under changes in the ambient excitation statistics. Mech. Syst. Signal Process. **45**(1), 207–224 (2014). https://www.sciencedirect.com/science/article/pii/S0888327013005645

23. Basseville, M., Abdelghani, M., Benveniste, A.: Subspace-based fault detection algorithms for vibration monitoring. Automatica **36**(1), 101–109 (2000). https://www.sciencedirect.com/science/article/pii/S000510989900093X

24. Basseville, M., Mevel, L., Goursat, M.: Statistical model-based damage detection and localization: subspace-based residuals and damage-to-noise sensitivity ratios. J. Sound Vibr. **275**(3), 769–794 (2004). https://www.sciencedirect.com/science/article/pii/S0022460X03009556

25. Étienne Balmès, Basseville, M., Bourquin, F., Mevel, L., Nasser, H., Treyssède, F.: Merging sensor data from multiple temperature scenarios for vibration monitoring of civil structures. Struct. Health Monit. **7**(2), 129–142 (2008). https://doi.org/10.1177/1475921708089823

26. Yan, A.M., Golinval, J.C.: Null subspace-based damage detection of structures using vibration measurements. Mech. Syst. Signal Process. **20**(3), 611–626 (2006). https://www.sciencedirect.com/science/article/pii/S0888327005000798

27. Zhu, M., McKenna, F., Scott, M.H.: Openseespy: Python library for the opensees finite element framework. SoftwareX **7**, 6–11 (2018). https://www.sciencedirect.com/science/article/pii/S2352711017300584

28. Greiner, B.: Operational modal analysis and its application for SOFIA telescope assembly vibration measurements. Universität Stuttgart, Institut für Raumfahrtsysteme, Ph.D. thesis (2009)

29. Groth, E.B., Clarke, T.G.R., Schumacher da Silva, G., Iturrioz, I., Lacidogna, G.: The elastic wave propagation in rectangular waveguide structure: determination of dispersion curves and their application in nondestructive techniques. Appl. Sci. **10**(12) (2020). https://www.mdpi.com/2076-3417/10/12/4401

30. Aggarwal, C.C.: Neural Networks and Deep Learning. Springer, Cham (2018). https://doi.org/10.1007/978-3-319-94463-0

31. Raschka, S.: Python Machine Learning. Packt Publishing - ebooks Account (2015). http://www.amazon.com/exec/obidos/redirect?tag=citeulike07-20&path=ASIN/1783555130